small
NANO MICRO

Polymer-Protected Sub-2-nm-Nanogap Fabrication for Biological Sensing in Near-Physiological Conditions**

*Huijuan Zhang, Robert J. Barsotti, Chee-Leong Wong, Xuejia Xue, Xiaogang Liu, Francesco Stellacci, and John T. L. Thong**

There has been considerable interest in developing methods for rapid and sensitive detection of biological molecules such as DNA and proteins in biodefense and drug-discovery applications.[1,2] Fluorescence-based optical-detection methods are widely used in various settings, but these methods require labeling of the target molecules and generally exhibit a relatively low detection sensitivity and thus are not suitable for rapid and inexpensive detection of small quantities of target molecules.[3–6] Electrical detection schemes have recently gained significant attention because they are label-free and capable of rapidly detecting minuscule quantities of molecules.[7–15] Among electrical-based detection methods, nanogap devices that comprise a pair of electrodes with separations on the order of nanometers have been intensively investigated.[11–20] Several approaches, including nanoimprinting,[15] electron-beam lithography,[21,22] dip-pen lithography,[23] shadow masking,[24] electrochemical etching/deposition,[25] and thermally-assisted electromigration of lithographically defined narrow thin wires,[26–31] have been demonstrated to fabricate sub-100-nm gaps. However, these nanogaps have limitations for biological detection in aqueous solutions under near-physiological conditions (i.e., high ionic strength)[32] as the current flowing through the gap can be orders of magnitude smaller than the parallel ionic current flow between the macroscopic electrodes.[33,34] A very recent publication by Huang et al. describes an approach to fabricate polymer-protected gap electrodes but with relatively large-gap junctions (25–100 nm) that could potentially be used to address this ionic-current issue.[35]

Here we present a facile approach to the fabrication of sub-2-nm nanogaps with self-aligned conformal hole structures in the overlying polymer layer that significantly minimize non-specific binding of biomolecules and nanoparticles. In addition, we show that the background ionic-noise current through these nanogaps in electrolytes of high salt concentration is reduced by two orders of magnitude. We also demonstrate that the self-aligned polymer-protected nanogap devices with substantial reduction in parasitic ionic currents could be used for rapid and inexpensive sensing of DNA strands in aqueous solutions without the constraints typically associated with conventional nanogaps.

In a typical procedure, a 100-nm-thick poly(methyl methacrylate) (PMMA) layer is first coated on a Au electrode fabricated with a constriction as shown in Scheme 1A (3D view). During the application of a slow voltage ramp (1 mV per 7 s), the electrode gradually breaks down due to electromigration, opening a sub-2-nm gap while simultaneously forming an overlying PMMA hole structure precisely located on the newly-formed nanogap (Scheme 1B, 3D view). We will show that the formation of the hole structure can be attributed to heat-induced ablation as illustrated in Scheme 1 (side view). We will present reasons to believe that the increase in voltage induces a Joule heating at the constriction site, which causes the polymer to expand locally and reflow when the temperature exceeds the polymer's glass transition point, forming a protuberance on top of the constriction site (Scheme 1, step i; side view). Subsequently, localized thermal expansion of the polymer leads to a buckling event that forms a dome-shaped structure between the PMMA and the Au electrode (Scheme 1, step ii; side view). The high tensile stress developed on the PMMA layer and the rapid increase in local temperature as electromigration progresses lead to polymer ablation at the

[*] Prof. J. T. L. Thong
Department of Electrical and Computer Engineering
National University of Singapore
117576 (Singapore)
E-mail: elettl@nus.edu.sg

H. Zhang
Advanced Materials for Micro- and Nano-Systems Program
Singapore–MIT Alliance 117576
(Singapore)

Dr. R. J. Barsotti, Prof. F. Stellacci
Department of Materials Science and Engineering
Massachusetts Institute of Technology
Cambridge, MA 02139 (USA)

C.-L. Wong
Centre for IC Failure Analysis and Reliability
Department of Electrical & Computer Engineering
National University of Singapore
4 Engineering Drive 3, 117576 (Singapore)

X. Xue, Prof. X. Liu
Department of Chemistry
National University of Singapore
117543 (Singapore)

[**] This work is supported by the Singapore–MIT Alliance and the National University of Singapore. H. Zhang is grateful to the Singapore–MIT Alliance for support through a fellowship.

Supporting Information is available on the WWW under http://www.small-journal.com or from the author.

DOI: 10.1002/smll.200900938

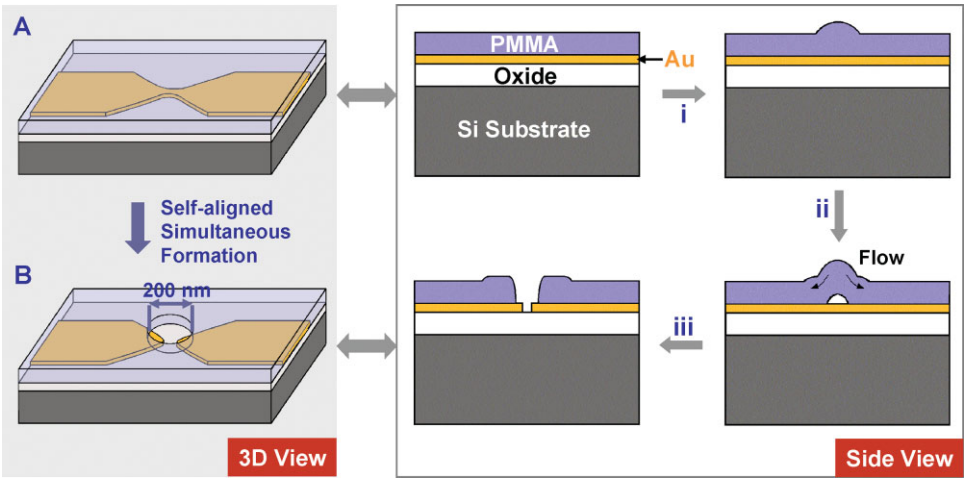

Scheme 1. Self-aligned formation of a nanogap with a conformal PMMA hole nanostructure. Left) 3D view of the device before (A) and after (B) electrical stressing. Right) Side view of the device formation process. i) PMMA expansion at the constriction site upon Joule heating. ii) Formation of a dome structure induced by a buckling event. iii) Simultaneous formation of a sub-2-nm gap and a hole nanostructure by PMMA ablation.

constriction site, resulting in the formation of a hole structure on top of the nanogap (Scheme 1, step iii; side view). The hole feature is about 200 nm in diameter (full width at half maximum, FWHM) and precisely aligned to the nanogap. Such alignment is particularly difficult to achieve by conventional electron-beam lithography due to variability in the position of the nanogap that eventually opens as a result of the electromigration process.

As proof-of-concept experiments, we have successfully fabricated 44 self-aligned conformal hole structures out of 50 attempts while all 50 tries have sub-2-nm nanogaps. The as-fabricated nanostructures were first characterized by atomic force microscopy (AFM). Figure 1a shows a typical AFM topography image of the PMMA hole structure with a diameter of 200 nm at the constriction site. In contrast, failed attempts resulted in formation of protuberant features as shown in Figure 1b. The morphology of the nanogap formed simultaneously via the thermally assisted electromigration at the pre-patterned constriction site was further examined by scanning electron microscopy (SEM) (Figure 1c). A typical current–voltage (I–V) curve for nanogap formation and the resulting tunneling I–V characteristics are shown in Figure 1S (Supporting Information). The tunneling current I through a metal–vacuum–metal gap is proportional to

$$\exp\left(-2\sqrt{\frac{2m(\Phi - V)}{\hbar^2}}\, d\right) \qquad (1)$$

where d is the gap distance, V is the applied voltage, and Φ is the work function of the gold electrodes.[28–30] The sizes of the gap are in the range of 1.1 ± 0.11 nm as determined by tunneling current measurements. Due to the electromigration process in a polycrystalline electrode, the nanogap is formed at an indeterminate location along a wider crack,[36] depending on the particular sample, and tunneling occurs through the nanogap representing the closest points between two electrodes. The formation of the wider crack followed by the tunneling nanogap is shown in Figure 2S (Supporting Information). To confirm the formation of PMMA hole nanostructure directly on top of the nanogap, the nanogap device modified with 3-aminopropyl triethoxysilane (APTS) was immersed in a solution of citrate-stabilized Au nanoparticles of ≈20-nm diameter.[37] The PMMA layer was then stripped off by acetone and the vicinity of the nanogap examined by SEM. As anticipated, Au nanoparticles were assembled in a circle centered on the nanogap as shown in Figure 1d, indicating that the PMMA hole nanostructure is well-aligned with the nanogap. The size (≈120 nm) of the nanoparticle aggregate patch is smaller than the FWHM diameter of the PMMA hole structure as determined from the

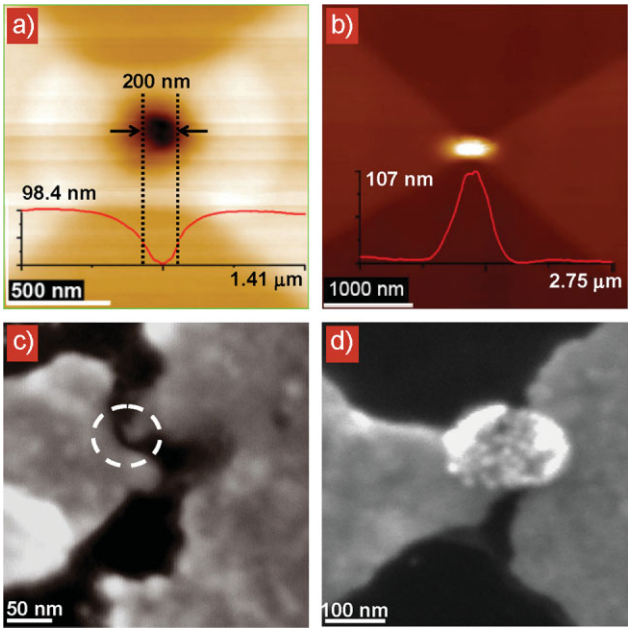

Figure 1. a) Topography image of a self-aligned hole by AFM and the height profile of the PMMA hole structure. b) Topography image of a PMMA protuberance by AFM and its height profile. c) SEM micrograph of a typical nanogap marked by a dashed circle. d) SEM micrograph of Au nanoparticles assembled at the nanogap templated by the PMMA hole.

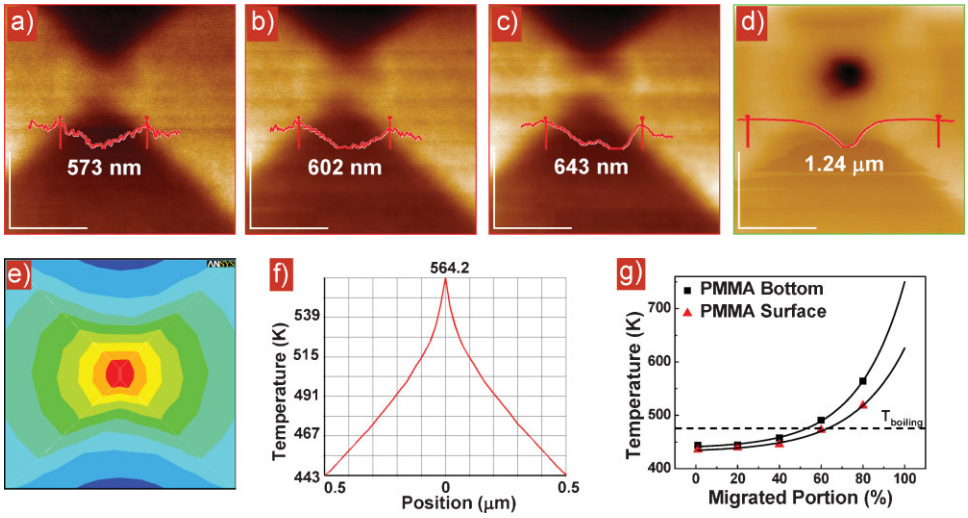

Figure 2. a–d) A series of real-time AFM images of a bowtie electrode coated with PMMA upon applying electric stressing. A line profile along the bowtie and separation between peaks shows progressive PMMA reflow with time (scale bars are 500 nm). e) Simulated temperature map of the PMMA layer indicating temperature transitions from hot (red color) to cold (blue color). f) The corresponding temperature profile of the PMMA surface at the constriction site. g) Temperature plots of the PMMA bottom layer (black square) and top surface (red triangle) versus the portion migrated at the constriction site: 0% = no migration, 100% = final nanogap formation. The solid lines are fitted data and the dashed line is the boiling temperature of PMMA. The projected temperature of the PMMA is as high as 750 K at the bottom and 626 K at the surface.

AFM line scan partly due to the probable sloping of the polymer profile, partly due to artifacts in size determination of deep holes through AFM tips, and partly due to hydrophobic repulsion of charged Au particles from the PMMA walls.

To support the thermal-ablation-induced hole formation mechanism, the volume changes of the PMMA layer before and after electrical stressing were analyzed by real-time AFM imaging. During electrical stressing, the bowtie structure covered by the PMMA was continuously scanned by AFM. 1.5 μm × 1.5 μm scan images of the constriction site were captured at 1-min intervals. Noticeable topographical changes occurred in the time interval of 133 to 136 min (Figure 2a–d). The volume loss of 1.84×10^{-3} μm^3 upon hole formation was determined from differential AFM measurements, implying a thermal-ablation event occurred in the polymer layer. A similar calculation was performed for the volume change of the PMMA protuberance shown in Figure 1b, which yielded a volume increase of 0.046 μm^3. Such a large volume increase is ≈200 times greater than expected from thermal expansion alone (PMMA expansion coefficient $\alpha = 6.7 \times 10^{-4}$),[38] substantiating the formation of the dome-shaped structure at the constriction site as presented in Scheme 1. The temperature profiles of the PMMA layer and Au electrode were simulated by using the multi-physics simulation software ANSYS 10.0. The constriction site is considered to be progressively electromigrated as observed in Figure 2S and illustrated in Figure 3S (Supporting Information). At the start of electromigration, the electrode structure is as defined, and the temperature profile is simulated at 20%–80% reduction in the constriction width at intervals of 20% to model the temperature rise. As shown in Figure 2e and f, upon Joule heating the local temperature of PMMA at the constriction with 20% of the original width remaining is around 560 K. The local temperature is not only higher than the glass transition temperature ($T_g = 399$ K), but also the boiling point ($T_{boiling} = 473$ K) of PMMA, promoting the occurrence of the polymer ablation.[39] The simulated PMMA temperature agrees well with PMMA ablation experiments carried out by Luo et al.[40] Figure 2g is a plot of the simulated peak temperature versus the portion electromigrated. It should be noted that the local temperature of the PMMA increases rapidly in the course of electromigration.

Importantly, the self-aligned polymer-protected nanogap exhibits significantly reduced ionic current in an aqueous solution in the presence of high salt concentration. To validate the ionic-current-reduction capability, one bare nanogap and one PMMA-protected nanogap were tested in a phosphate buffer saline (PBS) solution (0.3 M NaCl, 10 mM NaH_2PO_4/Na_2HPO_4, pH 7). As shown in Figure 3a, the ionic current detected by the bare nanogap is 20 nA at 500 mV. In contrast, the PMMA-protected nanogap shows 0.1 nA at 500 mV. The hysteresis loop for the bare nanogap in the *I–V* curve can be attributed to the capacitance of the electrolyte solution. In addition, the PMMA-protected nanogap showed only subtle variations in ionic current at different salt concentrations (1, 0.3, and 0.1 M NaCl) (Figure 3b).

We further examined the polymer-protected nanogap for DNA-detection application in aqueous solutions. The exposed electrodes were first modified with a single-stranded oligonucleotide (capture strand **a**) and placed into a solution (0.3 M PBS buffer solution) of 15-nm Au nanoparticles modified with a different single-stranded oligonucleotide (probe strand **b**) (Figure 4a).[41,42] In the presence of a complementary target DNA (target strand **a'b'**), the nanogap device showed a marked increase in electrical conductance (Figure 4b). In contrast, with non-complementary target DNA the nanogap showed essentially unaltered electrical conductance as no Au nanoparticle assembled. Comparative SEM images of Au nanoparticle assembly on test samples with mismatched target and with complementary target are shown in Figure 4S (Supporting

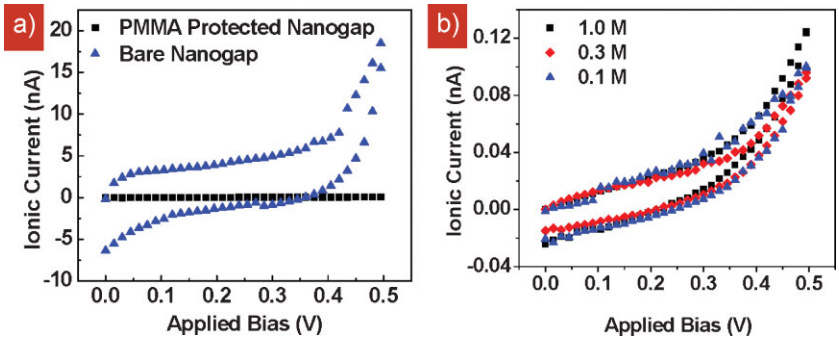

Figure 3. a) *I–V* characteristics of a bare nanogap and a nanogap with a self-aligned conformal PMMA hole (200-nm-diameter) in 0.3 M PBS buffer. b) *I–V* characteristics of a nanogap with a self-aligned conformal PMMA hole in 1, 0.3, and 0.1 M NaCl solution. Measurements were done at a voltage sweep rate of 5 mV per 50 ms.

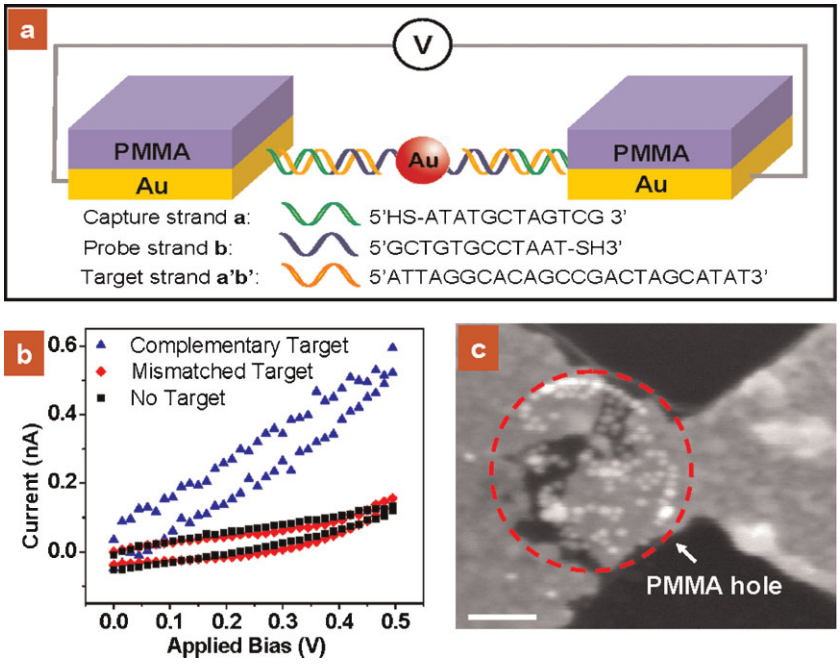

Figure 4. a) Schematic of target DNA detection by a detection system that comprises a PMMA-protected nanogap and oligonucleotide-modified Au nanoparticles. b) *I–V* characteristics of the nanogap before and after DNA hybridization in the presence of Au nanoparticles in a 0.3 M buffer solution. Measurements were done at a voltage sweep rate of 5 mV per 50 ms. c) SEM image of a nanogap showing nanoparticle assembly in the vicinity of the nanogap electrodes upon DNA hybridization. Note that the PMMA layer was removed by oxygen plasma for high-resolution SEM image and the dashed red circle indicates the approximate position of the original PMMA hole structure. The scale bar is 100 nm.

Information). The target DNA-induced electrical response is attributed to the controlled assembly of Au nanoparticles in the vicinity of the nanogap, thereby providing an additional current pathway. This was confirmed by SEM characterization of the nanogap, showing high density of nanoparticles precisely assembled into the electrode gap (Figure 4c). It should be noted that without the PMMA layer protection the measured ionic current ($\approx 10^{-8}$ A) through a bare nanogap device as shown in Figure 3a completely masks the electrical read-out signal ($\approx 10^{-10}$ A) in the event of DNA hybridization.

In conclusion, we have presented a novel approach to the fabrication of self-aligned PMMA-protected sub-2-nm nanogaps. The approach exploits a combination of electromigration and thermal-ablation techniques by utilizing PMMA-coated Au electrodes with a bowtie constriction. Importantly, the self-aligned polymer-protected ultra-small nanogaps exhibit two orders of magnitude reduction in parasitic ionic currents and thus offer markedly improved signal-to-noise ratio, which should find particularly useful applications for in situ biological detection directly in aqueous solutions under near-physiological conditions. We have demonstrated here the application for wet DNA sensing, focusing primarily on ionic-current reduction by the polymer hole. In fact, this application for DNA sensing has not reached the limit of the polymer-protected nanogap as the sub-2-nm nanogap was not fully exploited. It should be noted that the polymer-protected sub-2-nm nanogap is capable of capturing molecules, peptides, or DNA, which are much smaller than the 15-nm Au nanoparticles used here, and detecting/studying these molecules in aqueous solution.[43,44] Our efforts in this direction are currently underway.

Experimental Section

Fabrication of PMMA-protected nanogaps: To produce ultra-small nanogaps, electrode patterns with a weak bowtie junction were delineated in PMMA resist by electron-beam lithography on a 500-nm SiO_2-covered silicon die. A metal layer of 18-nm-thick Au and 1.5-nm-thick Ti (as adhesion layer) was thermally evaporated (BOC Edwards, Auto 306 Vacuum Evaporator) on the patterned die and lifted-off in acetone to create the Au electrode. This was followed by optical lithography using AZ5212 photoresist to define large bond pads (400 μm × 400 μm). A second layer of 150-nm-thick Au and 15-nm Ti was thermally evaporated and lifted-off to deposit the contact pads. An insulating polymer layer, in this case ≈100-nm-thick PMMA was spun on to coat the entire device. Next, a simple voltage sweep at 1 mV per 7 s was applied to the bowtie structure at room temperature using a Keithley 4200 parameter analyzer to stress the electrode till tunneling current was detected (when conductance $<2e^2/h$).[26] The surface

morphology of the polymer-protected nanogaps was examined by AFM (JEOL SPM 5200).

Attachment of Au nanoparticles by APTS: [37] Citrate-stabilized Au nanoparticles of ≈20 nm in diameter were purchased from SPI supplies and Structure Probe, Inc. A nanogap with a self-aligned hole structure at the constriction site was firstly immersed into 0.05% APTS in water for 10 min to form a self-assembled layer of APTS on the substrate. The substrate was then immersed in a solution of Au nanoparticles for 2 h to allow assembly of the nanoparticles and subsequently blow-dried with nitrogen. The presence of nanoparticles at the nanogap was examined by SEM (Philips XL 30 FEG).

Temperature-simulation model: The structure used was a trilayer model consisting of a PMMA layer (100-nm-thick), the Au electrode (20-nm-thick) and the underlying SiO_2 (500-nm-thick). The bottom SiO_2 layer was defined as the boundary condition due to a large thermal mass attributed to the Si substrate (500 μm). The electrical load was a voltage sweep from 0 to 1.2 V in steps of 1 mV per 7 s following the actual experimental conditions.

Functionalization of nanogap electrodes and Au nanoparticles: [41] All oligonucleotides were purchased from Sigma–Aldrich Ltd. Au nanoparticle (15-mm-diameter) solution was prepared following a literature method.[45] The 3′- or 5′-terminal disulfide of oligonucleotide strands were first cleaved by dithiothreitol (DTT) in a buffer solution (0.1 M phosphate, pH 8.0) for 2 h and purified with a NAP-5 column purchased from GE Healthcare Ltd. The Au colloid solution was then mixed with the purified thiol–DNA solution and left overnight. The concentration was gradually increased to 0.3 M NaCl, 10 mM NaH_2PO_4/Na_2HPO_4, pH 7 buffer (0.3 M PBS buffer) every 4 h. After 48 h the nanoparticles were centrifuged and redispersed in 0.3 M PBS buffer. The surface modification of nanogap electrodes with thiolated oligonucleotides was carried out via a similar procedure. For DNA detection, the nanogap substrate was immersed into a mixed solution of probe-DNA-functionalized Au nanoparticles (2 nM) and target DNA (1 μM; final target concentration). The device was then incubated at 65 °C for 20 min and slowly cooled down.

Keywords:
biological sensing · DNA detection · ionic current · nanogaps

[1] G. Ramsay, *Nat. Biotechnol.* **1998**, *16*, 40.
[2] M. I. Pividori, A. Merkoci, S. Alegret, *Biosens. Bioelectron.* **2000**, *15*, 291.
[3] S. P. Fodor, R. P. Rava, X. C. Huang, A. C. Pease, C. P. Holmes, C. L. Adams, *Nature* **1993**, *364*, 555.
[4] D. J. Lockhart, E. A. Winzeler, *Nature* **2000**, *405*, 827.
[5] C. C. Xiang, O. A. Kozhich, M. Chen, J. M. Inman, Q. N. Phan, Y. Chen, M. J. Brownsein, *Nat. Biotechnol.* **2002**, *20*, 738.
[6] X. Zhao, R. Tapec-Dytioco, W. Tan, *J. Am. Chem. Soc.* **2003**, *125*, 11474.
[7] D. J. Caruana, A. Heller, *J. Am. Chem. Soc.* **1999**, *121*, 769.
[8] S. M. Yang, C. Chang, T. I. Yin, P. L. Kuo, *Sens. Actuators, B* **2008**, *130*, 674.
[9] T. Sakata, M. Kamahori, Y. Miyahara, *Jpn. J. Appl. Phys.* **2005**, *44*, 2854.
[10] S. J. Park, T. A. Taton, C. A. Mirkin, *Science* **2002**, *295*, 1503.
[11] D. Porath, A. Bezryadin, S. Vries, C. Dekker, *Nature* **2000**, *403*, 635.
[12] S. W. Chung, D. S. Ginger, M. W. Morales, Z. Zhang, V. Chandrasekhar, M. A. Ratner, C. A. Mirkin, *Small* **2005**, *1*, 64.
[13] L. Moreno-Hagelsieb, P. E. Lobert, R. Pampin, D. Bourgeois, J. Remacle, D. Flandre, *Sens. Actuators, B* **2004**, *98*, 269.
[14] Y. T. Cheng, C. Y. Tsai, P. H. Chen, *Sens. Actuators, B* **2007**, *120*, 758.
[15] X. Liang, S. Y. Chou, *Nano Lett.* **2008**, *8*, 1472.
[16] M. M. Deshmukh, A. L. Prieto, Q. Gu, H. Park, *Nano Lett.* **2003**, *3*, 1383.
[17] G. S. McCarty, *Nano Lett.* **2004**, *4*, 1391.
[18] M. A. Reed, C. Zhou, C. J. Muller, T. P. Burgin, J. M. Tour, *Science* **1997**, *278*, 252.
[19] R. .J Barsotti, Jr, M. D. Vahey, R. Wartena, Y. M. Chiang, J. Voldman, F. Stellacci, *Small* **2007**, *3*, 488.
[20] S. Hashioka, M. Saito, E. Tamiya, H. Matsumura, *Appl. Phys. Lett.* **2004**, *85*, 687.
[21] M. D. Fischbein, M. Drndic, *Appl. Phys. Lett.* **2006**, *88*, 063116.
[22] D. L. Klein, P. L. McEuen, J. E. B. Katari, R. Roth, A. P. Alivisatos, *Appl. Phys. Lett.* **1996**, *68*, 2574.
[23] H. Zhang, S. W. Chung, C. A. Mirkin, *Nano Lett.* **2003**, *3*, 43.
[24] E. P. Poortere, H. L. Stormer, L. M. Huang, S. J. Wind, S. O'Brien, M. Huang, J. Hone, *J. Vac. Sci. Technol. B* **2006**, *24*, 3213.
[25] L. Qin, S. Park, L. Huang, C. A. Mirkin, *Science* **2005**, *309*, 113.
[26] D. R. Strachan, D. E. Smith, D. E. Johnston, T. H. Park, M. J. Therien, D. A. Bonnell, A. T. Johnson, *Appl. Phys. Lett.* **2005**, *86*, 043109.
[27] M. L. Trouwborst, S. J. van der Molen, B. J. van Wees, *J. Appl. Phys.* **2006**, *99*, 114316.
[28] D. R. Strachan, D. E. Smith, M. D. Fischbein, D. E. Johnston, B. S. Guiton, M. Drndic, D. A. Bonnell, A. T. Johnson, *Nano Lett.* **2006**, *6*, 441.
[29] T. Taychatanapat, K. I. Bolotin, F. Kuemmeth, D. C. Ralph, *Nano Lett.* **2007**, *7*, 652.
[30] T. Hayashi, T. Fujisawa, *Nanotechnology* **2008**, *19*, 145709.
[31] C. Y. Tsai, T. L. Chang, R. Uppala, C. C. Chen, F. H. Ko, P. H. Chen, *Jpn. J. Appl. Phys.* **2005**, *44*, 5711.
[32] N. Mano, H. H. Kim, Y. Zhang, A. Heller, *J. Am. Chem. Soc.* **2008**, *130*, 324.
[33] S. Seo, M. D. King, R. F. Young, L. B. Kish, M. Cheng, *Microelectron. Eng.* **2008**, *85*, 1484.
[34] B. Xu, P. Zhang, X. Li, N. Tao, *Nano Lett.* **2004**, *4*, 1105.
[35] Y. C. Lin, J. Bai, Y. Huang, *Nano Lett.* **2009**, *6*, 2234.
[36] C. Durkan, M. A. Schneider, M. E. Welland, *J. Appl. Phys.* **1999**, *86*, 1280.
[37] W. Chen, H. Ahmed, K. Nakazoto, *Appl. Phys. Lett.* **1995**, *66*, 3383.
[38] K. Wondraczek, J. Adams, J. Fuhrmann, *Macromol. Chem. Phys.* **2004**, *205*, 1858.
[39] O. Kahle, U. Wielsch, H. Metzner, J. Bauer, C. Uhlig, C. Zawatzki, *Thin Solid Films* **1998**, *313*, 803.
[40] C. Luo, X. Liu, R. Poddar, J. Garra, A. P. Gadre, E. V. Keuren, T. Schneider, R. White, J. Currie, M. Paranjape, *J. Micromech. Microeng.* **2006**, *16*, 580.
[41] X. Xue, F. Wang, X. Liu, *J. Am. Chem. Soc.* **2008**, *130*, 3244.
[42] W. Xu, X. Xue, T. Li, H. Zeng, X. Liu, *Angew. Chem. Int. Ed.* **2009**, *48*, 6849.
[43] X. Xue, W. Xu, F. Wang, X. Liu, *J. Am. Chem. Soc.* **2009**, *131*, 11668.
[44] X. Xiao, B. Xu, N. Tao, *Nano Lett.* **2004**, *4*, 267.
[45] J. J. Storhoff, R. Elghanian, R. C. Mucic, C. A. Mirkin, R. L. Letsinger, *J. Am. Chem. Soc.* **1998**, *120*, 1959.

Received: June 2, 2009
Revised: July 27, 2009
Published online: October 30, 2009

